

Article

# An Indirect Method for Monitoring Dynamic Deflection of Beam-Like Structures Based on Strain Responses

Wan Hong <sup>1,\*</sup> , Zheng Qin <sup>1</sup>, Kui Lv <sup>1</sup> and Xuan Fang <sup>2</sup>

<sup>1</sup> College of Civil Engineering, Nanjing Tech University, Nanjing 211816, China; 643433248@njtech.edu.cn (Z.Q.); 652081402041@njtech.edu.cn (K.L.)

<sup>2</sup> Nanjing Gongda Construction Technology Co., Ltd., Nanjing 211899, China; 91bluelemon@sina.com

\* Correspondence: w.hong@njtech.edu.cn; Tel.: +86-025-5813-9488

Received: 10 April 2018; Accepted: 15 May 2018; Published: 18 May 2018



**Abstract:** An indirect method for monitoring dynamic deflection of beam-like structures using strain responses measured by long-gauge fiber Bragg grating (FBG) sensors is proposed in this paper. Firstly, a theoretical derivation shows that structural deflection is in direct and linear relationship to long-gauge strain. Meanwhile, the method is suitable for structures with different boundary conditions and irrelevant to external loads. Secondly, the influence of boundary conditions, load type and sensor gauge length on the method is investigated by numerical simulation. Finally, an experiment of a simply supported beam subjected to dynamic loads was designed to verify the method. Experimental results show that both deflection time-history of arbitrary points of structures and deflection distribution along structures at a certain time can be obtained with high-precision. Therefore, the method presented can be a new alternative for the deflection evaluation and maintenance of engineering structures.

**Keywords:** deflection; fiber Bragg grating sensors; beam-like structures

## 1. Introduction

The ability to extract key parameters of existing structures using smart sensors attracted growing attention in past decades due to these parameters accurately reflecting structural in-service conditions. Such information is vital for decision-making in terms of maintenance and retrofitting. Among these performance parameters, deflection is a commonly used index. In the design of civil-engineering structures (bridges, buildings, tunnels, etc.), the deflection limit is usually utilized as a control index of structures when subjected to potential external loads. The deflection limit for structures is a mandatory index in most design codes to ensure structural safety.

It is essential to obtain deflection for the performance assessment of structures in operation. The methods to measure deflection are classified into direct and indirect methods. Displacement transducers are well-known tools for the direct measurement of structural deflection. Although this is a convenient method to measure deflection in a laboratory experiment due to perfect test conditions, it is hard to utilize this kind of sensor in practical engineering. In order to arrange this kind of sensor, the reference point is required, but it is difficult to find such reference point in real structures especially for long-span bridges and buildings. The global positioning system (GPS) is another direct method for measuring displacement and can be utilized in real structures [1]. Compared to flexural structures, the accuracy of GPS in a rigid structure which has relatively smaller deflection is still a concern. Recently, advanced techniques in other direct measurement tools have been developed. A new technique was developed by [2] for the displacement measurement of a flexible bridge based

on the digital image technique. The feasibility of vertical displacement measurement was investigated by [3] for bridges using charge-coupled device (CCD) cameras. In addition, [4] developed a method for the displacement measurement of buildings based on webcams. These image-processing methods are confronted with the problem of the influence of light when applied in on-line monitoring.

Indirect methods have also attracted growing attention. Among these techniques, deflection estimation using strain responses has been investigated by many researchers. The advantages of this concept are summarized as: (1) the reference point is not required; (2) various goals can be achieved using only one kind of sensor and costs can be reduced. According to the relationship of double integration between deflection and curvature, deflection can be estimated by curvature or strain [5]. In addition, the authors in [6,7] presented curvature function expressed by polynomial, and the coefficients in polynomial can be determined by regression analysis of experiment data. Once the curvature function is achieved, deflection can be estimated by double integral. Other relevant studies about deflection estimation using curvature can be found in [8–10]. For structures subjected to dynamic load, dynamic deflection can be estimated using dynamic strain. Dynamic strain is the numerical summation of the results of strain mode shapes multiplied by modal coordinates, while dynamic deflection is the numerical summation of the results of displacement mode shapes multiplied by modal coordinates. Hence dynamic deflection can be obtained by strain mode shapes [11–15]. Moreover [16], investigated the displacement estimation of a two-dimensional plate based on the modal approach.

The objective of this paper is to develop an improved moment-area method for the deflection estimation of engineering structures. The characteristics of the presented method are listed as: (1) a linear and direct relationship between strain and deflection is established to avoid error caused by the aforementioned double integral of curvature or transformation of response between time-domain and frequency-domain; (2) the method is suitable for both static and dynamic loads and external loads are irrelevant; (3) the method is applicable for different boundary conditions; (4) long-gauge strain sensors are utilized to ensure damage can be reflected and identified [17–22], and therefore the method can be reasonably extended to damaged structures. Firstly, the relationship between long-gauge strain and deflection was theoretically derived based on the improved moment-area method. Secondly, a numerical simulation was conducted, and the influence of boundary conditions, load type and sensor gauge length on the method was investigated. Finally, a simply supported beam subjected to dynamic loads was designed to verify the method. Experimental results show that both the deflection time-history of arbitrary points of structures and deflection distribution along structures at a certain time can be obtained with high precision.

## 2. Theoretical Background

The moment-area method [23] is commonly used to describe the relationship between the moment and deflection of structures. The moment and deflection curves of a simply supported beam subjected to an external load are illustrated in Figure 1. The span of the beam is denoted as  $L$ . Take point A as the reference point; tangent deflection  $\Delta$  is the distance between the deflection curve at point B and the tangent line of deflection curve at point A (shown in Figure 1). According to the principle of the moment-area method,  $\Delta$  can be expressed as:

$$\Delta = \int_A^B X_1(M(z)/EI) dz \quad (1)$$

in which  $M(z)$  represents moment at  $z$  and  $EI$  represents bending stiffness of the beam.  $X_1$  represents the distance between point B and differential  $dz$ .

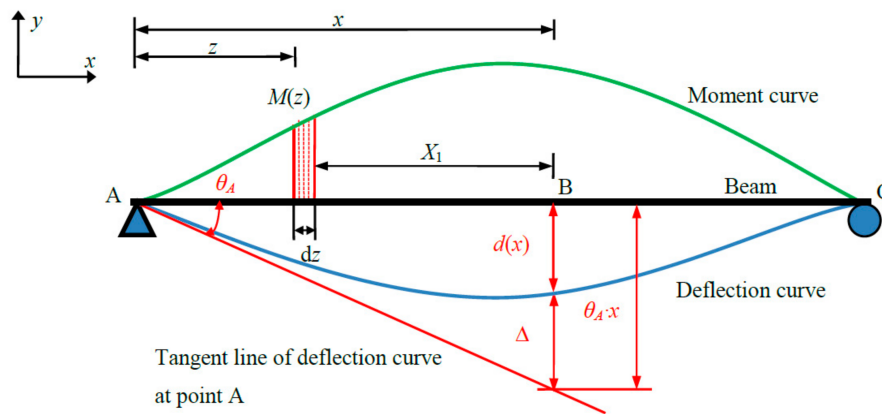


Figure 1. Principle of moment-area method.

The deflection of point B with the coordinate of  $x$  can be calculated by the moment distribution of the beam. From Figure 1, the deflection of point B can be expressed as:

$$d(x) = \theta_A x - \Delta = \theta_A x - \int_A^B (x - z)(M(z)/EI) dz \tag{2}$$

in which  $\theta_A$  represents rotating angle of point A.

Similarly, the distance between the deflection curve at point C and the tangent line of deflection curve at point A is equal to  $\theta_A L$ . Based on Equation (1),  $\theta_A$  can be calculated:

$$\theta_A = \frac{\int_A^C (L - z)(M(z)/EI) dz}{L} \tag{3}$$

Normally, Equation (2) is applicable when the moment distribution of the beam is known. The following section will derive the relationship between strain and deflection when the moment distribution (or external load) is unknown.

According to the physical equation, the sectional curvature of a certain point can be expressed as:

$$\frac{\varepsilon(z)}{h} = \frac{1}{\rho} = \frac{M(z)}{EI} \tag{4}$$

in which  $\varepsilon(z)$ ,  $h$  and  $1/\rho$  represent strain at point  $z$ , neutral axis height and sectional curvature, respectively. With sectional curvature as the connection between strain and moment, deflection at any point  $x$  can be calculated by measured strain in spite of the unknown load. On the basis of this connection, Equation (2) can be modified as:

$$d(x) = \theta_A x - \int_A^B (x - z)(\varepsilon(z)/h) dz \tag{5}$$

Generally, the improved moment-area method not only keeps the advantage of the moment-area method, but also requires no information about the position and type of external load. The general equation suitable for estimating both static and dynamic deflection can be achieved as:

$$d(x, t) = \theta_A(t)x - \int_A^B (x - z)(\varepsilon(z, t)/h) dz \tag{6}$$

in which  $\theta_A(t)$  is equal to  $\int_A^C (L - z)(\varepsilon(z, t)/h) dz/L$ .  $d(x, t)$  and  $\varepsilon(z, t)$  represent deflection of point  $x$  and strain of point  $z$  at time  $t$ , respectively.

Long-gauge fiber Bragg grating (LG-FBG) sensors can measure average strain over a certain length, and possess both static and dynamic measurement capacity [24]. It is assumed that a number of  $m$  long-gauge strain sensors (LGSSs) are installed on the structure. The average strain obtained by  $i$ th LGSS with the gauge length  $L_i$  is denoted as  $\bar{\epsilon}_i$  (Figure 2a).

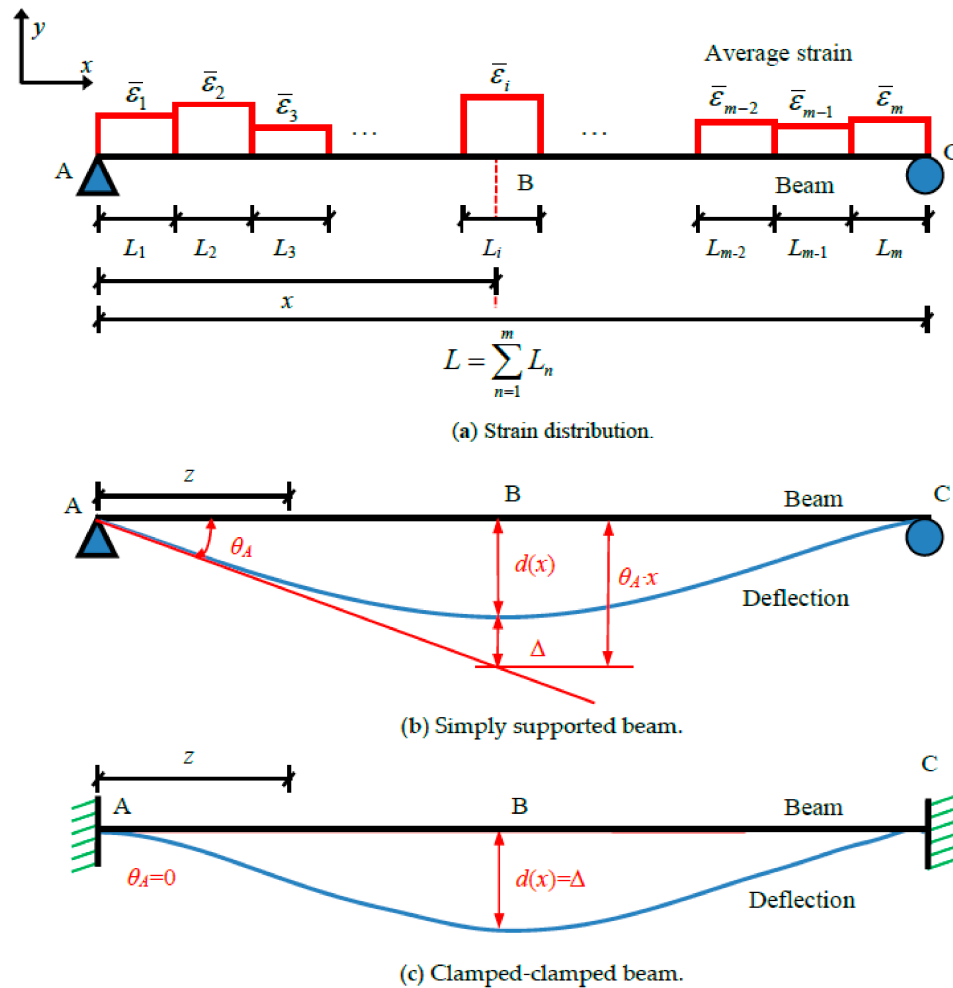


Figure 2. Deflection estimation for single-span beams.

Take a simply supported beam, for example (Figure 2b). The beam is free to rotate at support A. The rotating angle at point A is greater than zero and the value of  $\theta_A \cdot x$  is greater than  $d(x)$ . The deflection of point  $x$  of a simply supported beam at time  $t$  can be expressed as:

$$\begin{aligned}
 d(x, t) &= \theta_A(t)x - \int_0^x \frac{\epsilon(z, t)}{h} (x - z) dz \\
 &= \frac{x}{L} \sum_{n=1}^m \frac{\bar{\epsilon}_n(t)}{L_n} \int_{L_n} (L - z) dz - \left[ \sum_{n=1}^{i-1} \frac{\bar{\epsilon}_n(t)}{L_n} \int_{L_n} (x - z) dz + \frac{\bar{\epsilon}_i(t)}{L_n} \int_{\sum_{n=1}^{i-1} L_n}^x (x - z) dz \right] \quad (7)
 \end{aligned}$$

If  $\sum_{n=1}^{i-1} L_n < x \leq \sum_{n=1}^i L_n$ ,  $x$  lies in the region that  $i$ th LGSS covers.  $\sum_{n=1}^0 L_n$  is defined as zero.  $\int_{L_n}$  represents the integral within the region covered by  $n$ th sensor.  $\bar{\epsilon}_i(t)$  represents the dynamic strain at time  $t$  from the  $i$ th sensor.

For clamped-clamped beam (Figure 2c), the beam cannot rotate at support A and the rotating angle at support A is zero. In other words, the value of  $\theta_A \cdot x$  is zero and the value of  $\Delta$  is equal to

the value of  $d(x)$ . Therefore, the deflection of point  $x$  of a clamped-clamped beam at time  $t$  can be expressed as:

$$d(x, t) = - \int_0^x \frac{\varepsilon(z, t)}{h} (x - z) dz = - \left[ \sum_{n=1}^{i-1} \frac{\bar{\varepsilon}_n(t)}{L_n} \int (x - z) dz + \frac{\bar{\varepsilon}_i(t)}{\sum_{n=1} L_n} \int_{\sum_{n=1} L_n}^x (x - z) dz \right] \tag{8}$$

According to the aforementioned analysis, the method can be extended to continuous beams and other beams with different boundary conditions.

### 3. Verification by Numerical Simulation

#### 3.1. Model Building

Numerical simulations were conducted to validate the applicability of the method and discuss sensor optimization for the deflection calculation. Both single-span and three-span H-section steel beams were designed for finite-element analysis. The total length for the single-span and continuous beams was 8 m and 12 m, respectively. The supports of the single-span beams were divided into two types: simply supported and clamped-clamped. The material properties of these beams were as follows: elastic modulus  $E = 2.0 \times 10^{11}$  N/m<sup>2</sup>; linear mass density  $\rho = 7.8 \times 10^3$  kg/m<sup>3</sup>. More details about the models are illustrated in Figure 3.

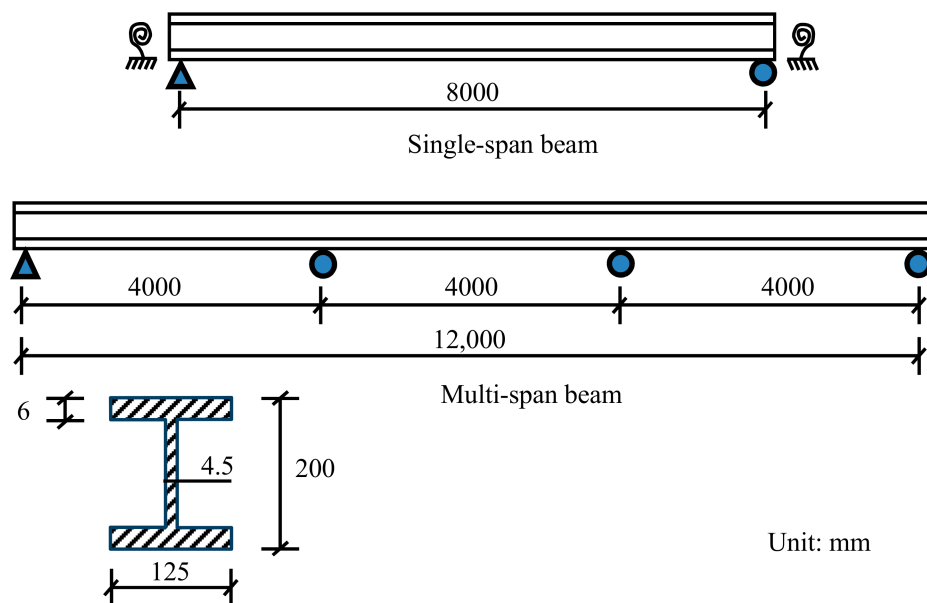


Figure 3. Different forms of simulation beams.

In the finite element analysis, the average strain measured by  $m$ th LGSS with the gauge length  $L_m$  can be extracted by:

$$\bar{\varepsilon}_m = \frac{h}{L_m} (\theta_i - \theta_j) \tag{9}$$

in which  $h$ ,  $\theta_i$  and  $\theta_j$  are neutral axis height, rotation angle of node  $i$  and  $j$ , respectively (Figure 4).

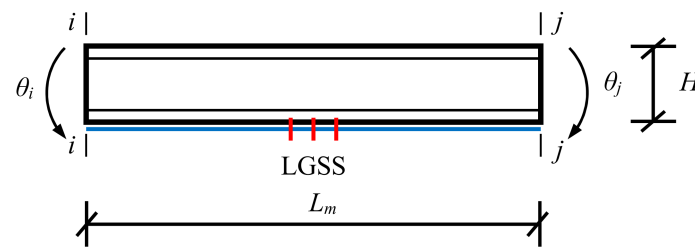


Figure 4. Strain and rotation angle.

### 3.2. Simulation Result Analysis

Using the software ANSYS (ANSYS, Inc., Canonsburg, PA, USA) [25], a simply supported beam, a clamped-clamped beam and three-span continuous beams are simulated. The applicability of the deflection calculation method for three loading cases was analyzed in these simulations. The average strain distribution along the beams (40 cm of sensor gauge length) was extracted using Equation (9).

Under the concentrated loads, the simply supported and clamped-clamped beams were under two point loads  $P_1$  and  $P_2$  at 1/4 and mid-span of the beams, respectively. The deflection distribution along the beams is shown in Figure 5a,b when  $P_1$  and  $P_2$  are equal to 2 kN and 4 kN, respectively. For Figure 5c, a point load of  $P = 10$  kN was exerted at the middle of the second span of the continuous beam. “Actual deflection” means directly extracted deflection from the nodes of finite element models. The relative errors between the predicted and actual deflection at the middle of the simply supported, clamped-clamped and three-span beams were 1.05%, 4.40% and 5.73%, respectively.

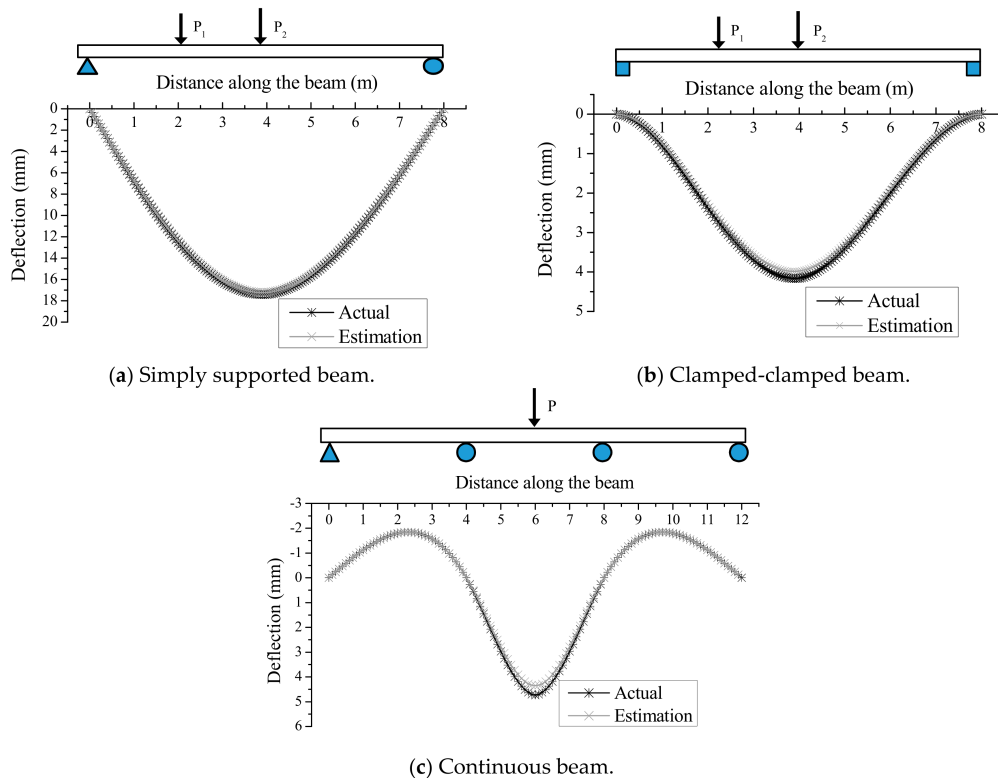


Figure 5. Deflection distribution along the different beams under point loads.

Under the even load, a uniform load  $q$  of 300 N/m is exerted on these beams. The vertical deflection distribution along the beams is demonstrated in Figure 6c. From the results of the analysis, the relative errors of deflection at mid-span of the simply supported and clamped-clamped beams are

0.9% and 4.4%, and the relative errors at the middle of each span of the continuous beam are 4.21%, 10.53% and 4.20%, respectively. The reason for the relative error of the second span is larger than those of other spans is that deflection of the second span under the uniform load is far less than that of other spans (Figure 6c).

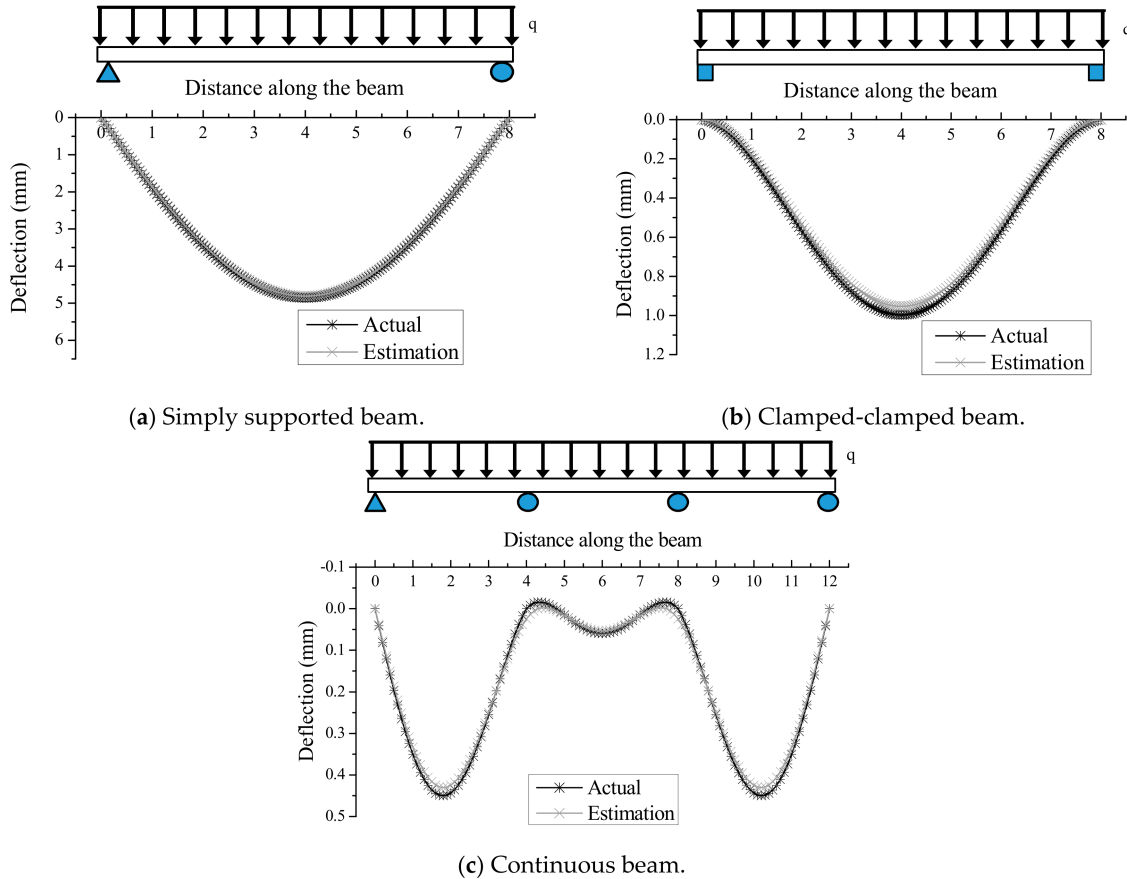


Figure 6. Deflection distribution along the different beams under uniform loads.

According to the simulation, the presented method is applicable to diverse forms of beams and different types of static loads. Generally, the relative error between the actual and predicted deflection for simply supported beams is less than those of clamped-clamped and continuous beams. This could be a result of the actual strain distribution having been substituted by average strain distribution in the method, and the relative error between the actual and average strain near the support is relatively larger for clamped-clamped and continuous beams subjected to the hogging moment. However, the relative error can be reduced by decreasing the gauge length of sensors near supports according to actual precision requirements.

Under the dynamic moving load, a double-axle vehicle load with the speed of 18 km/h and wheelbase of 0.4 m are exerted on these beams, and the weight of front and rear axles is 5 kN and 10 kN, respectively. Typical strain-time histories are demonstrated in Figure 7, and time-varying deflection at 1/4 span and mid-span is illustrated in Figure 8.

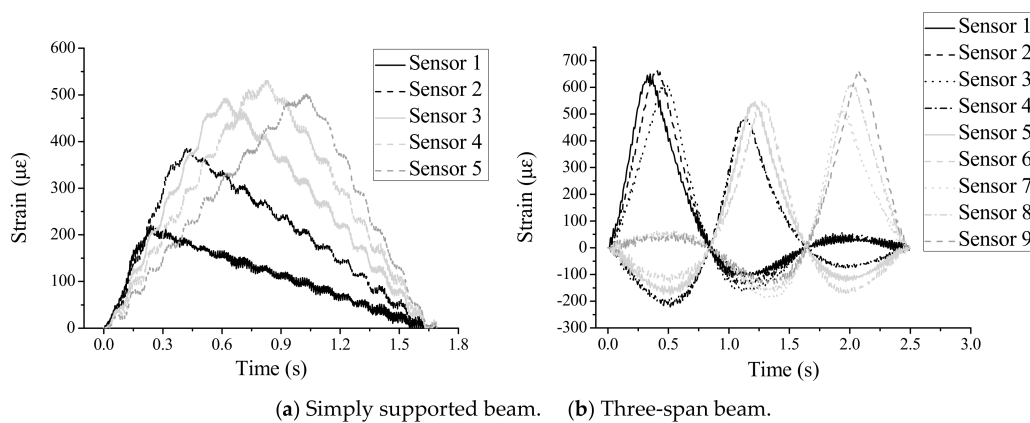


Figure 7. Typical strain-time histories of structures under dynamic moving loads.

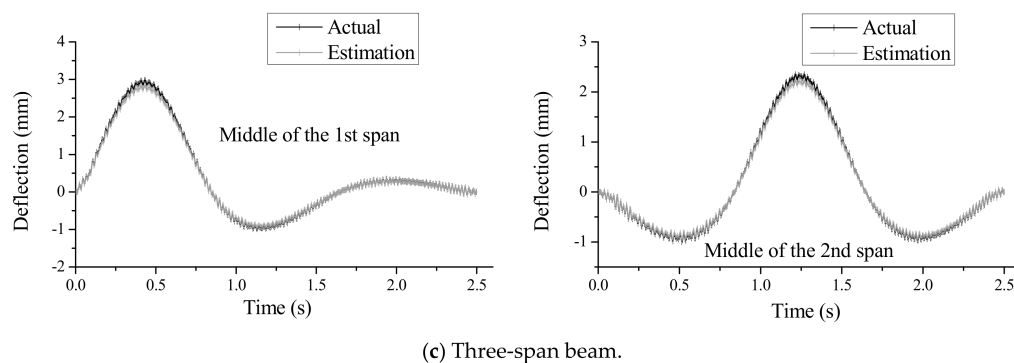
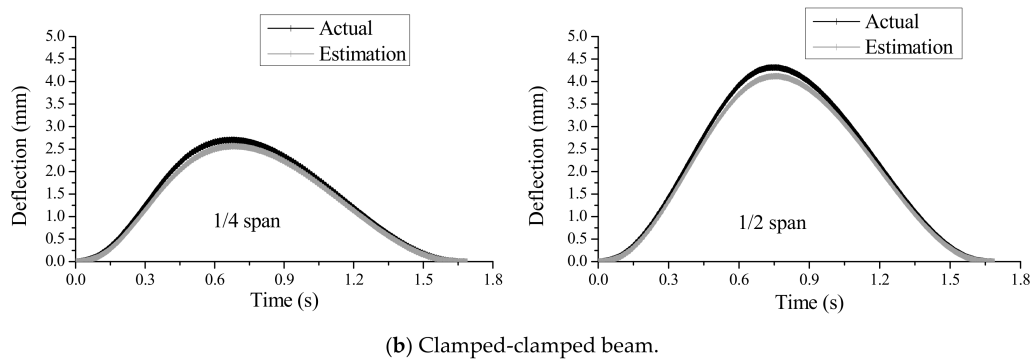
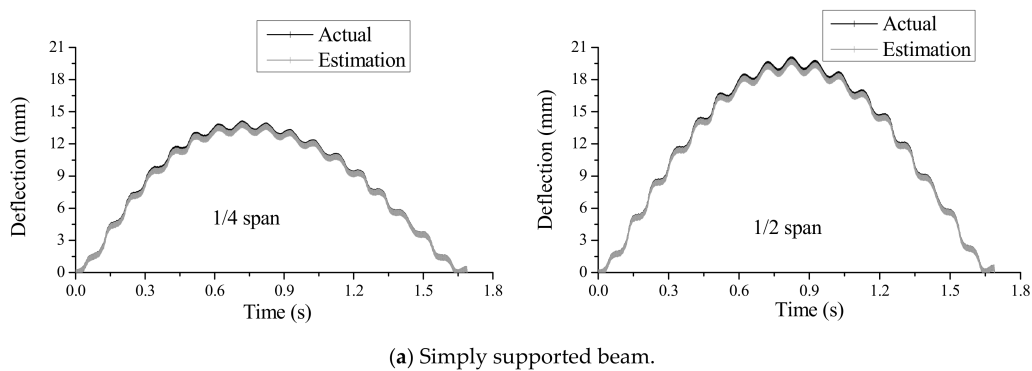


Figure 8. Time-varying deflection of structures under dynamic moving loads.

The applicability of the method under dynamic loads is verified based on transient analysis. During the process of a vehicle passing through the structure, the maximum relative error of deflection estimation of the simply supported beam is less than 1% and 2% at mid-span and 1/4 span, respectively. At time  $t = 0.65$  s, the relative errors of deflection at mid-span and 1/4 span are 5.03% and 5.40% for the clamped–clamped beam, respectively. For the continuous beam, the relative error of deflection at the middle of the first span is 4.80% at time  $t = 0.47$  s, while the error is 5.21% at the middle of the second span at time  $t = 1.28$  s.

### 3.3. Sensor Optimization

The purpose of sensor optimization is to help owners reach a balance between cost and precision requirements in real application. Take a simply supported beam under dynamic moving load for example, four samples are set for comparative analysis: (1)  $n = 80$ ,  $L_m = 0.1$  m; (2)  $n = 40$ ,  $L_m = 0.2$  m; (3)  $n = 20$ ,  $L_m = 0.4$  m; (4)  $n = 10$ ,  $L_m = 0.8$  m. The sensor number and sensor length are denoted as  $n$  and  $L_m$ , respectively. All sensors are distributed by being set on the bottom of the beam. The comparison results of these samples are illustrated in Figure 9.

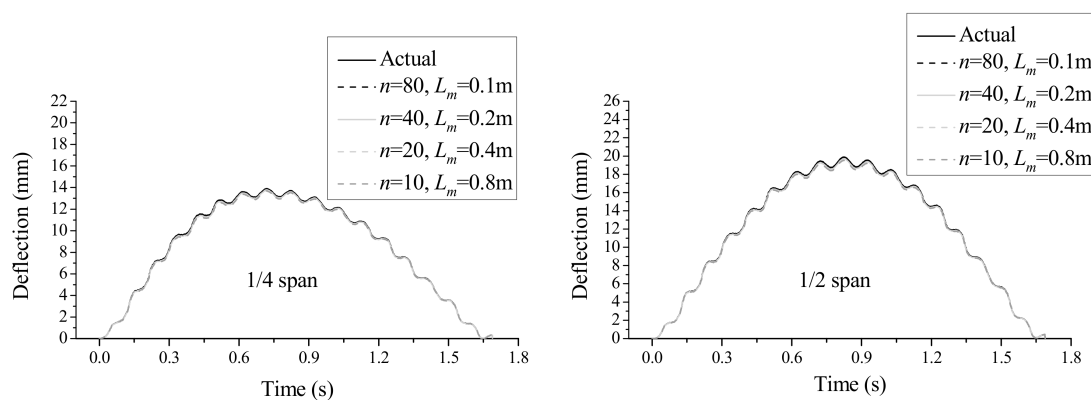


Figure 9. Results of sensor optimization.

Higher calculation accuracy will be obtained when more sensors (or smaller sensor length) are set due to the fact that average strain from LGSSs is closer to actual strain if sensor length is relatively smaller. Based on the analysis, the relative errors of deflection at mid-span at time  $t = 0.814$  s are 0.93%, 0.98%, 1.16% and 1.89% for samples (1) to (4), respectively. Obviously, this shows that the shorter the gauge length is, the higher the estimation accuracy is. Sensors can be optimized according to the balance between economic cost and accuracy requirements.

## 4. Verification by Experiment

### 4.1. Introduction of Fiber-Packaged Long-Gauge Fiber Bragg Grating (FBG) Sensors

Basalt fiber-packaged FBG sensors are utilized in the experiment. The design and manufacturing of fiber-packaged FBG sensors are demonstrated in Figure 10. A single packaged sensor is mainly composed of two parts: sensing section and anchoring points. The plastic separation tube outside the bare FBG makes sure the average strain between two anchoring points can be measured, and the length of the separation tube indicates the sensing length. In addition, basalt fibers outside the separation tube can guarantee the durability of sensors. It is noteworthy that basalt fibers should be reinforced with epoxy resin to produce a certain degree of stiffness, and pre-strain of the bare FBG can be transferred by this reinforced tube for the measurement of compressive strain. Detailed sensing properties about this kind of sensor can be found in [26].

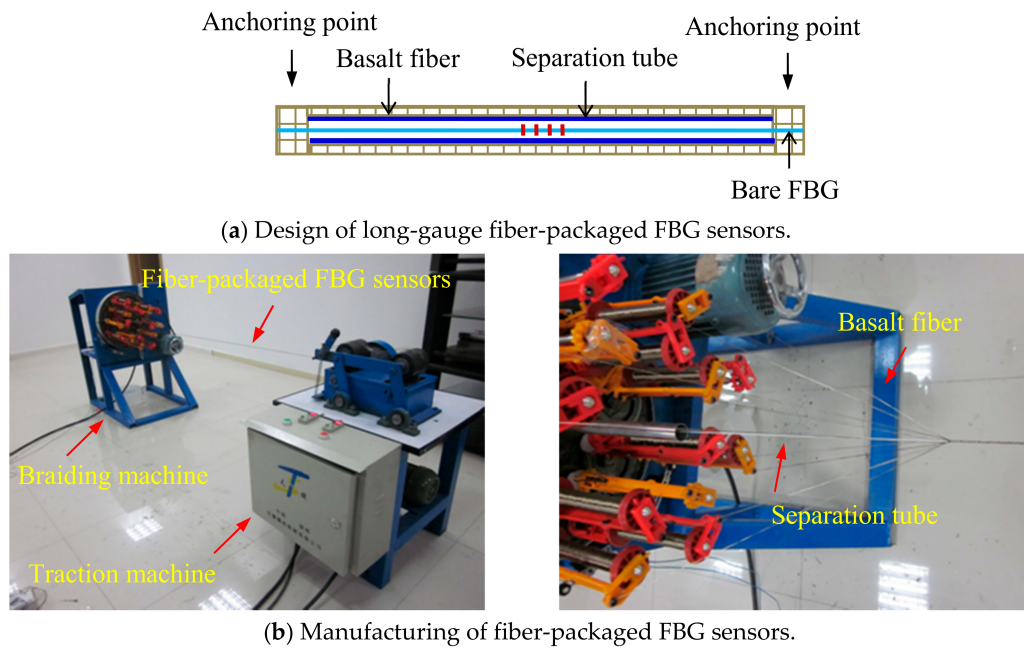


Figure 10. Design and manufacturing of fiber-packaged fiber Bragg grating (FBG) sensors.

#### 4.2. Experimental Setup

A simply supported steel beam was employed to validate the effectiveness of the improved moment-area method. The elastic modulus and density of the steel were  $E = 200$  GPa and  $\rho = 7800$  kg/m<sup>3</sup>, respectively. The cross section parameters of the specimen were: width of 100 mm and height of 12 mm. The overall length and net span of the simply supported beam were 2700 mm and 2400 mm, respectively. Seven basalt fiber-packaged FBG sensors (namely E1 to E7) were arranged on the bottom side of the test beam, of which the gauge length was 30 cm. The center of the first sensor (E1) was 30 cm from the left support. Three laser-displacement meters (namely L1 to L3) were also deployed for comparison. L1 and L3 were installed at 1/4 and 3/4 span of the test beam, respectively. L2 was arranged at mid-span of the test specimen. Detailed information about the test beam is provided in Figure 11.

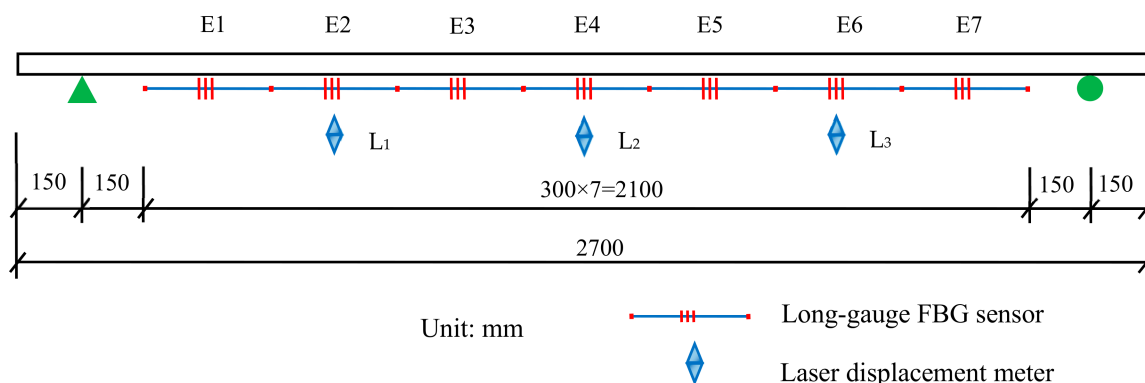


Figure 11. Experimental setup and sensor placement.

The test site overview of the specimen is shown in Figure 12a. It is noteworthy that a new form of support was applied to constrain the vertical displacement of supports. Considering vibration load, these supports made it approach the practical situation. More details of supports are shown in Figure 12b.

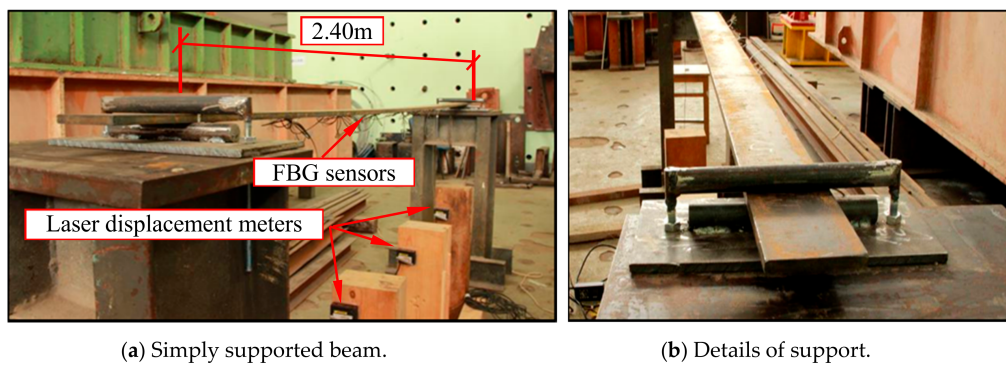


Figure 12. Experimental details.

#### 4.3. Analysis of Experimental Results

The loading types in this experiment include hammer excitation and vibration under sudden release of initial displacement. The typical strain time-history curves under the condition of single hammering and multiple hammering are shown in Figure 13. The deflection time-history at any position of the beams can be obtained using the aforementioned moment-area method. Furthermore, the deflection distribution along the beams at a certain time can also be achieved.

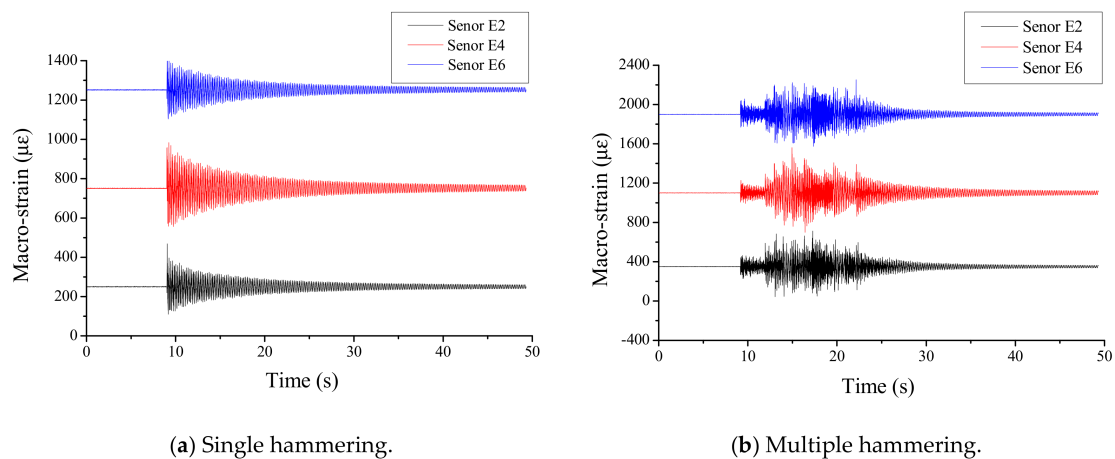


Figure 13. Typical long-gauge strain time-history curves.

The sampling frequency of FBG-based LGSSs (interrogator of SM130 from Micron Optics) and laser displacement meters is 100 Hz. Strain responses from each FBG sensor and displacement responses from each meter were simultaneously acquired. Taking 1/4 span, mid-span and 3/4 span of the beam as examples, deflection comparisons between the estimated results (Equation (7)) and directly measured results by laser displacement meters are shown in Figure 14. These figures show the time-varying deflection from  $t = 0$  s to  $t = 13$  s as well as the expanded one from  $t = 1$  s to  $t = 3$  s. From these expanded figures, it was found that the trend of the calculated deflection changing versus time was the same as the directly measured one. The errors between the calculated and measured deflection at the first peak (positive) and second peak (negative) were about 5.92% and 6.78% for 1/4 span of the beam. At mid-span, the errors between the calculated and the measured deflection were about 4.87% and 2.27% for the first and second peaks. At 3/4 span, the errors between the calculated and the measured deflection were about 5.30% and 7.76% for the first and second peaks. Generally, the relative errors of peak values can be controlled within about 10%. It is worth noting that “prediction” in Figure 14 means the results estimated using strain response, and “test results” means the results directly measured by laser displacement meters.

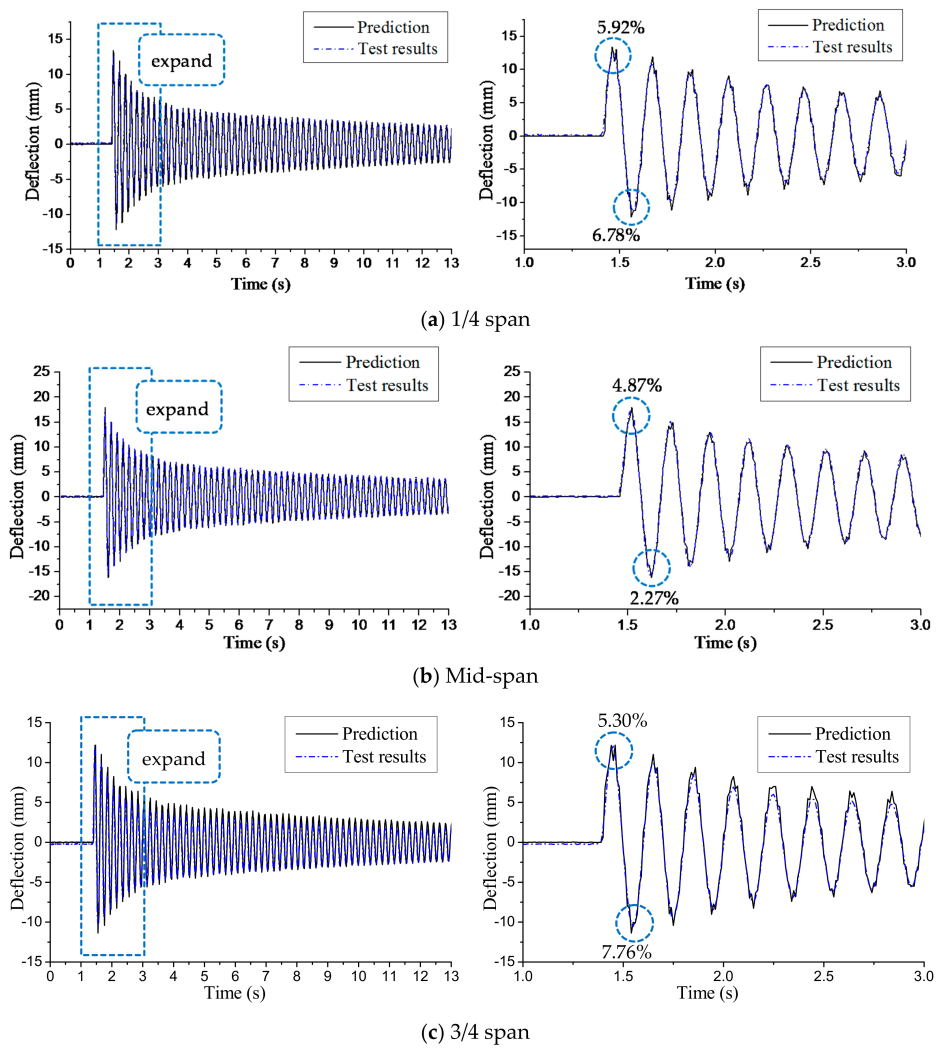


Figure 14. Comparison results of the beam under single hammering.

The deflection distribution along the length of the beam at a certain time can also be calculated using Equation (7). Typical calculated deflection shapes of the beam at different times are demonstrated in Figure 15.

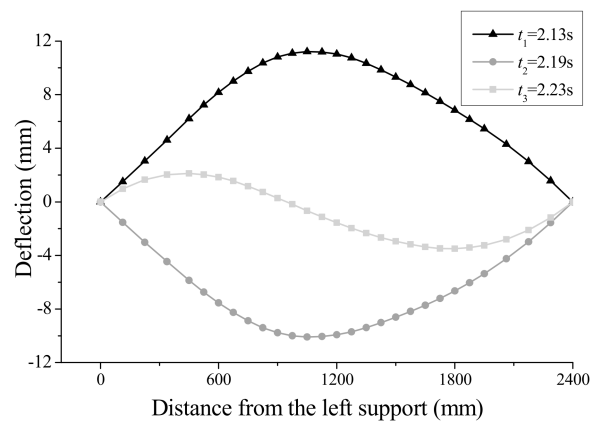


Figure 15. Calculated deflection shapes of the beam at different times.

Excitation in terms of the sudden release of initial vertical displacement of about 60 mm was also exerted at mid-span. When the initial vertical displacement was removed suddenly, strain and deflection responses were obtained with the beam vibrating. Similarly, the deflection changing with time at any position on the beam can be calculated using strain responses. Take calculated deflection at 1/4 span, mid-span and 3/4 span as examples, the comparison results for the estimated and measured deflection are shown in Figure 16. The calculated time-varying deflection tallies with the test result from Figure 16. The relative errors for the maximum values of deflection at 1/4 span, mid-span and 3/4 span of the beam are below 5%. On the whole, the deflection accuracy under excitation of the sudden release of vertical displacement is slightly better than that under hammering. It can be explained that the beam under excitation of the sudden release of vertical displacement mainly vibrates at low-frequency, which results in the error between the measured average strain and actual strain being relatively smaller compared to the excitation of hammering.

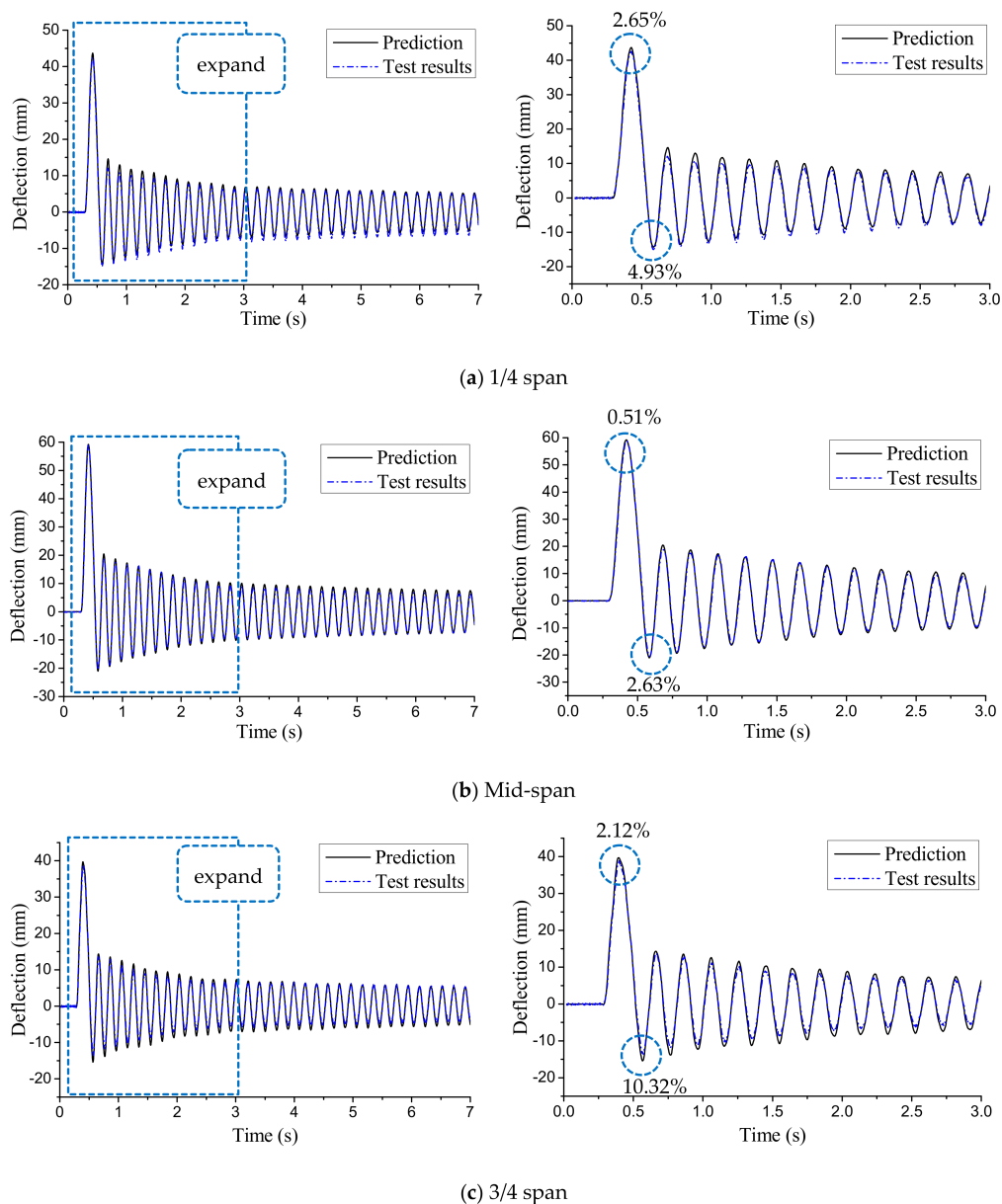


Figure 16. Comparison results of the beam under sudden release of initial displacement.

Meanwhile, the beam was also excited by repeatedly hammering. Take the time-varying deflection at mid-span, for example; the comparison results between the calculated and measured deflection of the beam under multiple hammering are illustrated in Figure 17. It is clear that the beam was hammered nine times on the basis of peaks of the deflection time history. The calculated deflection agrees well with the directly measured one when the beam was subjected to multiple hammering. Based on the aforementioned analysis, the method is applicable to different types of excitation.

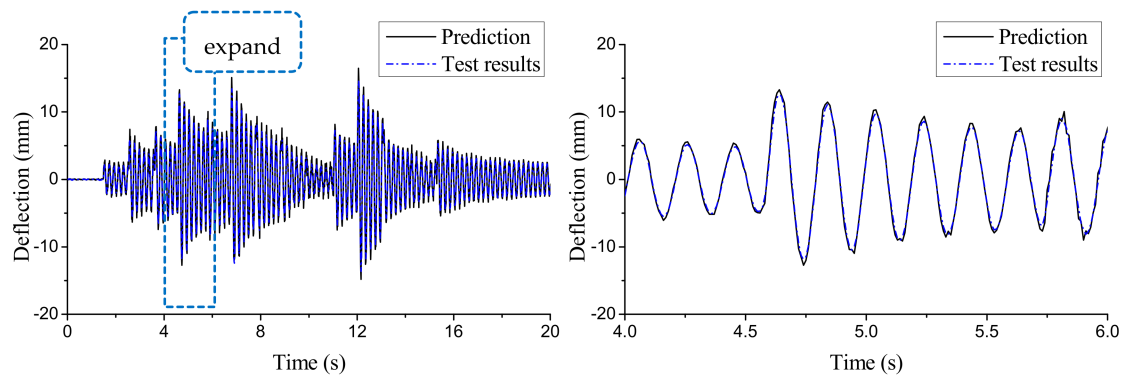


Figure 17. Comparison results of the beam under multiple hammering.

#### 4.4. Discussion

Based on the aforementioned analysis, deflection distribution along structures can be determined by strain distribution along them, and a linear and direct relationship exists between them. Thus, the double integration of curvature which can magnify the measurement error is not required in this method. LGSS can cover damage and reflect structural non-linearity, and hence the method can be reasonably extended to damaged structures. Compared to LGSSs, traditional “point” strain sensors will be confronted with an accuracy problem for deflection estimation of damaged structures due to the fact that damage will not be reflected by such “point” sensors unless such damages are covered. In addition, the aforementioned analysis is based on unknown external loads, and the sensor number or gauge length can be optimized if the external load is known.

#### 5. Conclusions

In this paper, an improved moment-area method for estimating structural deflection based on long-gauge FBG sensors is presented. Some conclusions can be summarized as:

- (1) A linear and direct relationship between strain and deflection is theoretically established, and the method is irrelevant to external loads and suitable for both static and dynamic loads.
- (2) Numerical simulation results show that the method is applicable for different boundary conditions, and sensors can be optimized according to the balance between economic cost and accuracy requirements.
- (3) Experimental results demonstrate that both deflection time-history of arbitrary points on the structures and deflection distribution along the structures at a certain time can be obtained with high precision.

**Author Contributions:** W.H. proposed the research and wrote the paper; Z.Q. and K.L. performed the experiments and analyzed the data; X.F. performed the numerical simulations and analyzed the data.

**Acknowledgments:** The paper was supported by grants from National Natural Science Foundation of China (Grant No. 51508269), Natural Science Foundation of Jiangsu Province (Grant No. BK20150957) and University Science Research Project of Jiangsu Province (Grant No. 15KJB580007).

**Conflicts of Interest:** The authors declare no conflict of interest.

## References

1. Fujino, Y.; Murata, M.; Okano, S.; Takeguchi, M. Monitoring system of the Akashi Kaikyo Bridge and displacement measurement using GPS. *Proc. SPIE* **2000**, *3995*, 229–236.
2. Lee, J.J.; Shinozuka, M. Real-time displacement measurement of a flexible bridge using digital image processing techniques. *Exp. Mech.* **2006**, *46*, 105–114. [[CrossRef](#)]
3. Chan, T.H.; Ashebo, D.B.; Tam, H.Y.; Yu, Y.; Chan, T.F.; Lee, P.C.; Perez Gracia, E. Vertical displacement measurements for bridges using optical fiber sensors and CCD cameras—a preliminary study. *Struct. Health Monit.* **2009**, *8*, 243–249. [[CrossRef](#)]
4. Park, J.W.; Lee, J.J.; Jung, H.J.; Myung, H. Vision-based displacement measurement method for high-rise building structures using partitioning approach. *NDT&E Int.* **2010**, *43*, 642–647.
5. Kim, N.S.; Cho, N.S. Estimating deflection of a simple beam model using fiber optic Bragg-grating sensors. *Exp. Mech.* **2004**, *44*, 433–439. [[CrossRef](#)]
6. Kang, D.; Chung, W. Integrated monitoring scheme for a maglev guideway using multiplexed FBG sensor arrays. *NDT&E Int.* **2009**, *42*, 260–266.
7. Chung, W.; Kim, S.; Kim, N.S.; Lee, H.U. Deflection estimation of a full scale prestressed concrete girder using long-gauge fiber optic sensors. *Constr. Build. Mater.* **2008**, *22*, 394–401. [[CrossRef](#)]
8. Kim, S.W.; Kang, W.R.; Jeong, M.S.; Lee, I.; Kwon, I.B. Deflection estimation of a wind turbine blade using FBG sensors embedded in the blade bonding line. *Smart Mater. Struct.* **2013**, *22*, 125004. [[CrossRef](#)]
9. Glaser, R.; Caccese, V.; Shahinpoor, M. Shape monitoring of a beam structure from measured strain or curvature. *Exp. Mech.* **2012**, *52*, 591–606. [[CrossRef](#)]
10. Bassam, A.; Ansari, F. A strain monitoring approach for estimating lateral displacements of concrete columns under seismic excitations. *J. Intell. Mater. Syst. Struct.* **2016**, *27*, 71–80. [[CrossRef](#)]
11. Foss, G.C.; Haugse, E.D. Using modal test results to develop strain to displacement transformations. In Proceedings of the 13th International Modal Analysis Conference, Nashville, TN, USA, 13–16 February 1995; pp. 112–118.
12. Li, C.J.; Ulsoy, A.G. High-precision measurement of tool-tip displacement using strain gauges in precision flexible line boring. *Mech. Syst. Sig. Process.* **1999**, *13*, 531–546. [[CrossRef](#)]
13. Wang, Z.C.; Geng, D.; Ren, W.X.; Liu, H.T. Strain modes based dynamic displacement estimation of beam structures with strain sensors. *Smart Mater. Struct.* **2014**, *23*, 125045. [[CrossRef](#)]
14. Kim, H.I.; Kang, L.H.; Han, J.H. Shape estimation with distributed fiber Bragg grating sensors for rotating structures. *Smart Mater. Struct.* **2011**, *20*, 035011. [[CrossRef](#)]
15. Kang, L.H.; Kim, D.K.; Han, J.H. Estimation of dynamic structural displacements using fiber Bragg grating strain sensors. *J. Sound Vib.* **2007**, *305*, 534–542. [[CrossRef](#)]
16. Rapp, S.; Kang, L.H.; Han, J.H.; Mueller, U.C.; Baier, H. Displacement field estimation for a two-dimensional structure using fiber Bragg grating sensors. *Smart Mater. Struct.* **2009**, *18*, 025006. [[CrossRef](#)]
17. Ansari, F. Fiber optic health monitoring of civil structures using long gauge and acoustic sensors. *Smart Mater. Struct.* **2005**, *14*, S1. [[CrossRef](#)]
18. Hong, W.; Wu, Z.; Yang, C.; Wu, G.; Zhang, Y. Finite element model updating of flexural structures based on modal parameters extracted from dynamic distributed macro-strain responses. *J. Intell. Mater. Syst. Struct.* **2015**, *26*, 201–218. [[CrossRef](#)]
19. Sigurdardottir, D.H.; Glisic, B. Neutral axis as damage sensitive feature. *Smart Mater. Struct.* **2013**, *22*, 075030. [[CrossRef](#)]
20. Hong, W.; Cao, Y.; Wu, Z. Strain-based damage-assessment method for bridges under moving vehicular loads using long-gauge strain sensing. *J. Bridge Eng.* **2016**, *21*, 04016059. [[CrossRef](#)]
21. Philips Adewuyi, A.; Wu, Z.; Kammrjuman Serker, N.H.M. Assessment of vibration-based damage identification methods using displacement and distributed strain measurements. *Struct. Health Monit.* **2009**, *8*, 443–461. [[CrossRef](#)]
22. Glisic, B. Influence of the gauge length on the accuracy of long-gauge sensors employed in monitoring of prismatic beams. *Meas. Sci. Technol.* **2011**, *22*, 035206. [[CrossRef](#)]
23. Hibbeler, R.C. *Structural Analysis*, 8th ed.; Prentice Hall: Upper Saddle River, NJ, USA, 2011; pp. 316–317.
24. Li, S.; Wu, Z. Development of distributed long-gauge fiber optic sensing system for structural health monitoring. *Struct. Health Monit.* **2007**, *6*, 133–143. [[CrossRef](#)]

25. ANSYS. *ANSYS 14.0*; ANSYS: Canonsburg, PA, USA, 2011.
26. Hong, W.; Wu, Z.S.; Yang, C.Q.; Wan, C.F.; Wu, G.; Zhang, Y.F. Condition assessment of reinforced concrete beams using dynamic data measured with distributed long-gage macro-strain sensors. *J. Sound Vib.* **2012**, *331*, 2764–2782. [[CrossRef](#)]



© 2018 by the authors. Licensee MDPI, Basel, Switzerland. This article is an open access article distributed under the terms and conditions of the Creative Commons Attribution (CC BY) license (<http://creativecommons.org/licenses/by/4.0/>).